Structure and Electronic Properties of Electrochromic NiO Films

D. A. Wruck[a] **and M. Rubin**

Lawrence Berkeley Laboratory, University of California, Berkeley, California 94720

ABSTRACT

Nickel oxide films were deposited by reactive RF magnetron sputtering. Optical and electrochemical characterization showed strong electrochromic activity under certain deposition conditions. X-ray diffraction and infrared absorption measurements indicate that the films are polycrystalline NiO and that the bulk crystal structure does not change upon oxidation and reduction. Electronic conduction in the films and charge storage at the NiO|electrolyte interface were studied by dc resistance and ac impedance measurements. The infrared measurements and x-ray photoelectron spectroscopy were used to characterize changes in surface composition. We interpret the experimental results as follows: electrochromic activity requires a porous, granular NiO film with excess oxygen at the grain surfaces. The film is reduced by the transfer of protons from water molecules to oxygen ions at the solid surface, and the film is oxidized by the transfer of protons from the solid surface to hydroxyl ions in solution.

The electrochemistry of hydrous nickel oxide has long been of interest due to its role as the active material on nickel battery electrodes,[1-5] and more recently, there has been much interest in the electrochromic behavior of nickel oxide thin films.[6-19] Potential applications for the films include adjustable-reflectance mirrors for automobiles and adjustable-transmittance windows for automobiles or buildings.[20,21] Nickel oxide is a promising alternative to the more widely studied tungsten oxide, but the fundamental mechanism of electrochemical coloration is uncertain. Even the coloring species is unknown, making the choice of ion conductors for devices difficult. We do know that the films undergo a redox reaction with a nearly transparent reduced state and a dark brown or black oxidized state. The optical changes are induced by small transfers of charge (about 20 mC/cm^2) in a cell with an alkaline electrolyte solution.

The electrochromic behavior is associated with the Ni(II)/Ni(III) couple, and the half-cell reaction is usually written as[1-5,21,22]

$$Ni(OH)_2(s) + OH^-(aq) \leftrightarrow NiOOH(s) + H_2O + e^-$$

Here "nickel oxide" will be used in a general sense to include hydrous forms such as hydroxides and oxyhydroxides. It is thought that the current at the solid|liquid interface is due to proton transfer between the solid surface and the OH^- and H_2O species in the solution, but the detailed mechanism of the proton transfer is not yet understood. The chemistry can be complicated by electrode porosity, variations in the structure of the oxide, oxygen gas evolution, and impurities trapped in or on the oxide. Although they apparently involve the same fundamental chemistry, the hydrous oxide layer on a battery electrode is typically operated in the range 30-100% Ni(III) oxide,[23] while an electrochromic film is typically operated in the range 0-10% Ni(III) oxide.

Electrochromic nickel oxide films can be grown by several techniques, including electrodeposition, vacuum evaporation, and sputter deposition. The film structure depends on the method of preparation. Films deposited from aqueous solutions of Ni salts have been studied by x-ray diffraction,[22] electron microscopy,[9,22] Raman scattering,[24] and x-ray absorption fine structure (EXAFS).[25] The samples tend to have porous structures with average grain sizes ≤100 nm. Polycrystalline β-$Ni(OH)_2$ films (brucite crystal structure, JCPDS file 14-117) and poorly crystallized α-$Ni(OH)_2$ films can be prepared by deposition from solution. Electron microscopy[13] and Raman scattering[12,18] studies of water-deposited electrochromic nickel oxide films have indicated that the films are polycrystalline NiO (NaCl crystal structure, JCPDS file 4-835). There may be hydroxylation of the film surface, and the electrochemical behavior of the film may be connected to excess oxygen compared to the formula value. Stoichiometric green NiO is chemically inactive, but oxygen-rich, polycrystalline black NiO can be chemically reactive. Moreover, in powder samples, the excess oxygen has been found to reside in the surface layers of the crystallites.[1,26]

We have previously reported on the effect of deposition parameters on sputtered electrochromic NiO films.[19] In this paper, we use x-ray diffraction and infrared (IR) absorption to give a more complete characterization of the structure of the films. Electronic transport and optical absorption in the films are investigated, and the film surface composition is studied with x-ray photoelectron spectroscopy. We propose that the electrochromism of the NiO films is derived from the hydroxylated grain surfaces, and the similar behavior of the NiO and $Ni(OH)_2$ films can be traced to the similar structure of the alkaline electrolyte|solid interface.

Experimental Methods

Film preparation and structure.—Electrochromic NiO films were deposited by RF magnetron sputtering of a Ni target in 28.5 mTorr Ar + 1.5 mTorr O_2. Further details of the film preparation process have been reported elsewhere.[19] The films studied here were grown on unheated substrates; a thermocouple indicated the substrate remained <80°C during deposition. Based on the zone model,[27] one predicts that the films have a porous structure consisting of columnar grains separated by voids. Films were grown on several materials, so the notation top layer/middle layer/substrate will be used to specify a sample. For example, NiO/Pt/fused silica is a NiO film atop a Pt film on a fused silica substrate, and NiO/glass is a NiO film on a glass substrate. Film thickness was determined with a Sloan Dektak IIA stylus profilometer.

The x-ray diffraction measurements were made in a Siemens Crystalloflex diffractometer with a Ni-filtered Cu K_α source. NiO/Pt/fused silica, NiO/SnO_2:F/glass, and NiO/In_2O_3:Sn (ITO)/glass samples were oxidized and reduced in 0.1*M* KOH, and the x-ray diffraction patterns were measured *ex situ*. The IR transmittance of NiO/NaCl samples and the IR reflectance of NiO/Pt/fused silica samples were measured in a Nicolet 5PC FTIR spectrometer. The Pt layer was about 0.3 μm thick and was opaque. The IR reflectance was measured at an angle of 30° to the normal, relative to a freshly deposited Pt/fused silica sample. The radiation was randomly polarized, and the samples were at room temperature in dry N_2. The NiO/Pt/fused silica samples were oxidized and reduced in 0.1*M* KOH, and the reflectance was measured *ex situ*. The near-normal reflectance was also measured in the visible and near-IR with a Perkin-Elmer Lambda 9 spectrophotometer to confirm that the NiO layer was coloring and bleaching.

[a] Present address: Nuclear Chemistry Division, L-396, Lawrence Livermore National Laboratory, Livermore, California 94550.

Electrical and electrochemical properties.—The NiO|metal contacts were initially tested to determine if they were ohmic. Ni, Pt, and Au contacts were tried, and each sample was prepared by sputter-depositing two 1 mm^2 disks of metal about 1 mm apart on 300 nm NiO/glass. The ac impedance of each metal|NiO|metal sample was measured with a Stanford Research Systems SR530 lock-in amplifier. The NiO resistance was ≈100 kΩ, and a depletion layer typically acts like a series capacitance of 0.1-1 μF/cm^2, so the impedance at frequencies below 1 kHz is sensitive to nonohmic contacts. However, the samples behaved as pure resistances over the measured range of 10-3000 Hz. This was also true for the tungsten carbide contacts of a four-point probe placed directly on a NiO film.

The observed behavior of the NiO|metal contacts can result from the highly granular structure of the films. There are many grain surface states at the NiO|metal interface, so the contact behavior is dominated by the flow of electrons between the grain surface states and the states at the Fermi level of the metal.[28] A related effect of the granularity is that the conductivity of the film can arise from conduction via the grain surface layers; the surface layer has an effective conductivity which is much larger than the bulk value.[26,29] The temperature dependence of the dc resistivity was determined by the van der Pauw method on NiO/glass samples.

Electrode potentials were controlled with a Pine RDE4 potentiostat, using a saturated calomel reference electrode (SCE) and a Pt counterelectrode. Electrode impedance measurements were made with a small-area electrode (apparent area 1.3×10^{-3} cm^2) prepared by depositing a 200 nm NiO film on the end of a Pt wire. The outer surface of the wire was masked with epoxy. A 1 mV rms ac potential was applied, and the ac current was measured with the lock-in amplifier. Initial measurements over the range 30-3000 Hz at fixed dc potentials indicated that the impedance could be modeled as a series resistance and capacitance. Further measurements were made at 100 Hz during a 1 mV/s sweep of the electrode potential.

Optical absorption and x-ray photoemission.—In order to avoid interference effects, a NiO/Au/glass sample was prepared with thin (≤30 nm) NiO and Au layers. The *in situ* transmittance of the sample was measured in a transparent cell in a Perkin-Elmer Lambda 9 spectrophotometer. The film was step-wise reduced at a constant current of 19 mA/cm^2, and the transmittance measurements were made at fixed steady-state potentials. The optical absorption cross section σ was calculated as

$$\sigma = \frac{e}{Q} \ln\left(\frac{T_b}{T}\right)$$

Here e is the elementary charge, Q is the transferred charge per unit area, T_b is the bleached-state transmittance, and T is the transmittance.

X-ray photoelectron spectroscopy (XPS) measurements were made in a PHI 5300 ESCA system. The x-ray source was Mg K_α, the x-ray beam was incident at 45°, and the axis of the electron energy analyzer was normal to the plane of the sample. Charge corrections were made by assigning 284.6 eV binding energy to the C 1s peak (from hydrocarbon contamination). Charge corrections were ≤0.2 eV for the data reported here.

For the XPS measurements, NiO films were grown on side-by-side ITO/glass substrates, oxidized or reduced in 0.1*M* KOH, then loaded into the XPS system through an air-lock chamber. There probably was some surface contamination as the samples were moved from the cell to the vacuum chamber; however, the samples were still bleached/colored when they were removed from the vacuum chamber. When returned to the cell, the bleached (reduced) samples were at roughly the same potential, and the colored (oxidized) samples had retained at least half their initial charge. Four of the bleached/colored pairs and five other individual samples were studied with XPS.

Results

The x-ray diffraction measurements indicate that the films are polycrystalline NiO (NaCl crystal structure, JCPDS file 4-835). Figure 1a shows the pattern for a 3.0 μm film on a fused silica substrate. The NiO (111) and (222) peaks are prominent, and the other NiO reflections are missing, which results from a preferred orientation of the (111) planes parallel to the film plane, and a random orientation of the grains about the direction normal to the film plane. The average grain size is ≈10 nm, as estimated from the peak widths.

X-ray diffraction patterns of the films grown on Pt/fused silica, SnO_2:F/glass, and ITO/glass show the NiO (111) and (222) peaks superposed on the pattern of the underlying film (Fig. 1b). The diffraction patterns were the same for the as-grown, bleached, and colored states. Up to 8 atomic percent (a/o) of the film was oxidized and reduced during these measurements, based on a transferred charge of 70 mC/cm^2 per μm of NiO. The barely resolved peak near $2\theta = 34°$ in Fig. 1a is due to the Cu K_β reflection from NiO (111), and the weak peak near $2\theta = 36°$ in Fig. 1b is attributed to a thin PtO layer.

The thickness of the NiO films did not change when the films were oxidized and reduced, within the resolution of the profilometer measurements (about 5%). The NiO layer thickness in several NiO/Pt/fused silica samples was determined to about 1% by fitting the interference peaks in the near-IR reflectance spectrum,[30] and again, there was no detectable change in thickness when the samples were oxidized and reduced.

The infrared absorption spectra of as-grown, bleached, and colored samples were essentially identical. Figure 2 shows the spectra near the NiO phonon frequencies for three films which are thin compared to the infrared wavelength. Strong absorption is expected at the transverse optical phonon frequency ω_T for radiation polarized in the film plane, and at the longitudinal optical phonon frequency ω_L for radiation polarized normal to the film plane.[31] The dashed lines in Fig. 2 mark ω_T and ω_L for NiO, as measured by neutron scattering.[32] The spectra show a dependence on film thickness because the NiO film is on Pt. The transverse electric field component is small near the metal surface, so the thinnest films have very weak absorption at ω_T. As the film thickness increases, a larger transverse electric field can be established in the film, and the absorption at ω_T grows relative to the absorption near ω_L. The upper band does not quite fall at ω_L, because for a porous film, individual-grain modes can become

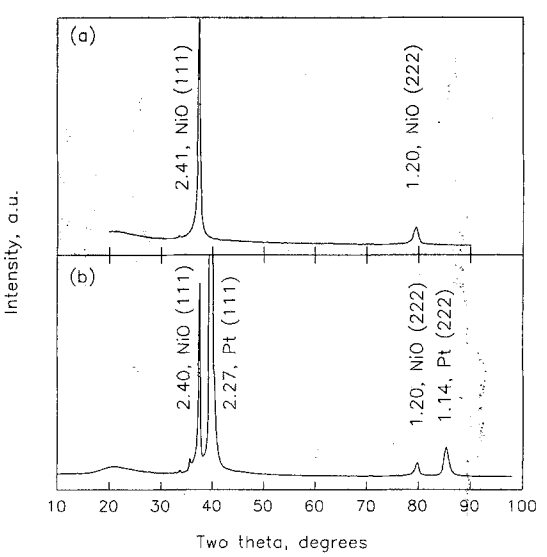

Fig. 1. X-ray diffraction patterns: (a) 3.0 μm NiO/fused silica sample; (b) 1.1 μm NiO/0.3 μm Pt/fused silica sample. The peaks are labeled with the assigned crystal planes and the measured plane spacings in angstroms.

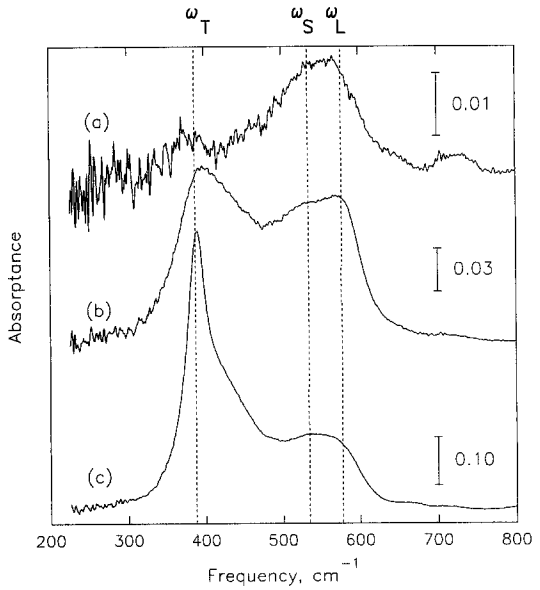

Fig. 2. Infrared absorption: (a) 0.20 μm NiO film on Pt; (b) 0.69 μm NiO film on Pt; (c) 1.08 μm NiO film on Pt. The dashed lines mark the TO (387 cm^{-1}) and LO (577 cm^{-1}) phonon frequencies of NiO, and the surface mode (534 cm^{-1}) for a NiO cylinder in air.

significant.[33] If a grain is modeled as a thin circular cylinder, strong absorption is expected at ω_T for radiation polarized parallel to the cylinder axis, and at frequency ω_S given by

$$\omega_s = \sqrt{\frac{\epsilon_0 + 1}{\epsilon_\infty + 1}}\,\omega_T$$

for radiation polarized in a plane normal to the cylinder axis. Hence ϵ_0 and ϵ_∞ are the dielectric constants of the cylinder, and it is assumed that the surrounding medium is air. In Fig. 2 the upper band falls between ω_L and ω_S calculated for a NiO cylinder. This may result from a distribution of crystallite shapes, or the crystallites may be arranged into chains which behave approximately as long cylinders with random orientations.[34]

A broad O-H stretch band near 3500 cm^{-1} and several bands in the 1100-1600 cm^{-1} region were seen for the NiO/Pt samples,[35] and these features show up clearly in the NiO/NaCl transmittance spectra (Fig. 3). The bands are present before the film is exposed to the electrolyte, and are attributed to adsorption of O_2 and water vapor. The O-H band can account for the 1600 cm^{-1} band, and the other bands in this range may arise from molecularly adsorbed O_2.[36,37] A

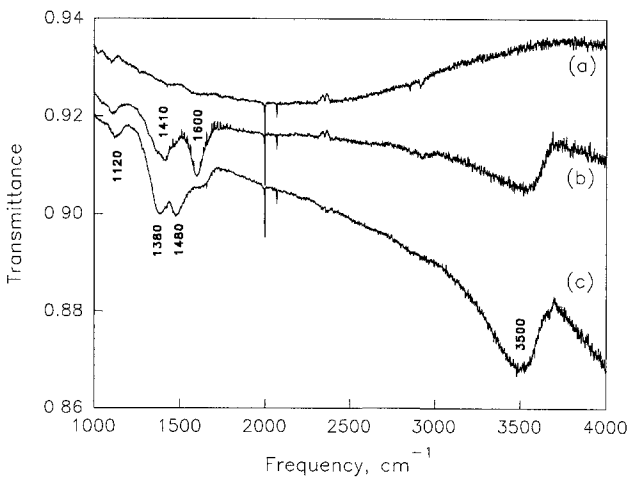

Fig. 3. Infrared transmittance: (a) uncoated NaCl substrate (displaced +0.01 units for clarity); (b) 50 nm NiO film on NaCl; (c) 100 nm NiO film on NaCl.

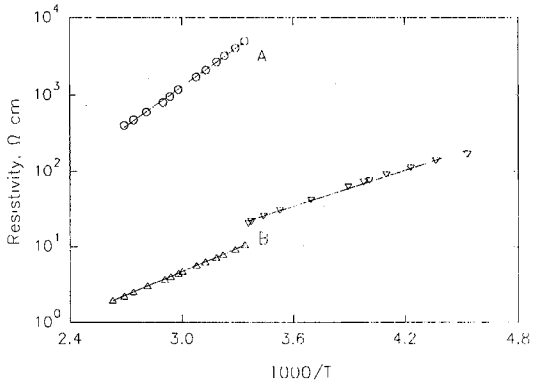

Fig. 4. DC resistivity of two NiO film samples. The activation energies determined from the indicated straight-line fits are: sample A, 0.32 eV; sample B, 0.21 eV ($T > 295$ K), 0.16 eV ($T < 295$ K).

change in the film thickness causes a shift of the bands in the 1400-1600 cm^{-1} range, which may be expected if the bands arise from collective modes of chains or layers that are larger on a thicker film.

Film samples were stored ≈1 year at room temperature with no apparent decrease in electrochromic response, but mild heat-treatments (1-2 h at 200°C) caused a decrease in the charge capacity and the corresponding optical absorption change of the films. The heat-treatments also increased the room temperature resistivity of the film, and the same results were obtained for heat-treatments in air and under vacuum (10^{-5} Torr). The temperature is too low for significant bulk diffusion in NiO, but O_2 and H_2O can be desorbed from NiO under these conditions.[38]

DC resistivity measurements on two NiO film samples are shown in Fig. 4. The magnitude of the resistivities and the activation energies suggest that the measurements are characteristic of conduction at the grain surfaces. The resistivity of crystalline NiO is 10^{13} Ω-cm, and the minimum activation energy for defects in bulk, undoped NiO is about 0.5 eV.[29] Sample B has a discontinuity at room temperature because the sample was first heated to 385 K, then cooled to 230 K, then heated to room temperature. The initial heating increased the room temperature resistivity.

Oxidation/reduction of a nickel oxide film is accompanied by a change in the film resistivity. An *in situ* measurement of a $Ni(OH)_2$ film using microelectrodes with ≈1 μm spacing has indicated a resistivity ≈30 Ω-cm for the oxidized state and ≈3×10^4 Ω-cm for the reduced state.[39] The following procedure demonstrated that, in a sputter-deposited film, the dc resistivity in the plane of the film remained ≥1 Ω-cm in the oxidized state. A 300 nm NiO/≈ 10 nm Ni/fused silica sample was prepared in the van der Pauw geometry, so the parallel combination of the NiO sheet resistance in the Ni sheet resistance (130 Ω) could be measured. The resistance did not change (within 0.5%) when the sample was oxidized and reduced; this places the stated limit on the dc resistivity.

Cyclic voltammograms for the electrodes used in the impedance measurements are shown in Fig. 5. The NiO electrode clearly displays the Ni(II)/Ni(III) current peaks, and in this potential range the Pt electrode is coated with a very thin passivating oxide. At 100 Hz, the electrode impedance (Fig. 6) is resolved into a resistance due primarily to electronic conduction in the NiO film and a capacitance from the double layer at the NiO/electrolyte interface. The resistance and capacitance change rapidly when the film is oxidized or reduced.

If the film is modeled as a homogeneous disk, the resistance axis in Fig. 6 corresponds to resistivity in the range 0 to 3×10^5 Ω-cm. Possible sources of the constant resistance for the oxidized film include the Pt|NiO contact or a ≈30 nm thick region of densely packed NiO grains which is chemically inactive. The resistance of the reduced film changes slowly with potential as the Ni(III) concentration in the solid phase is varied.

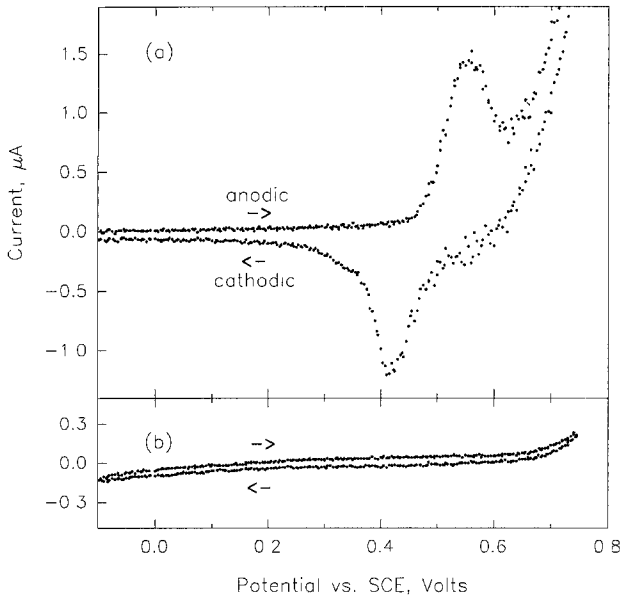

Fig. 5. Cyclic voltammograms of small-area electrodes used for the impedance measurements: (a) 200 nm NiO on Pt; (b) uncoated Pt. Apparent electrode area 1.3 × 10^{-3} cm^2; sweep rate 10 mV/s; electrolyte 1*M* KCl + KOH, pH 12.0.

In Fig. 6, the NiO capacitance is larger than the Pt capacitance because the true area of the NiO surface is likely to be larger than the true area of the Pt surface. The sharp changes in the capacitance of the NiO film electrode are caused by changes in the structure of the double layer. The direction of the change in capacitance is consistent with a reduced film which is mainly terminated in OH^- groups and an oxidized film which is mainly terminated in O^{2-} ions, such as would be expected for a proton transfer.

Using the capacitance plots or the cyclic voltammograms, the dependence of the electrode potential on electrolyte pH can be followed, and the result is a shift of −90 mV per pH unit.[35] This indicates that the electrochemistry is more complex than is represented in Eq. 1, which predicts a shift of −59 mV per pH unit. Similar potential/

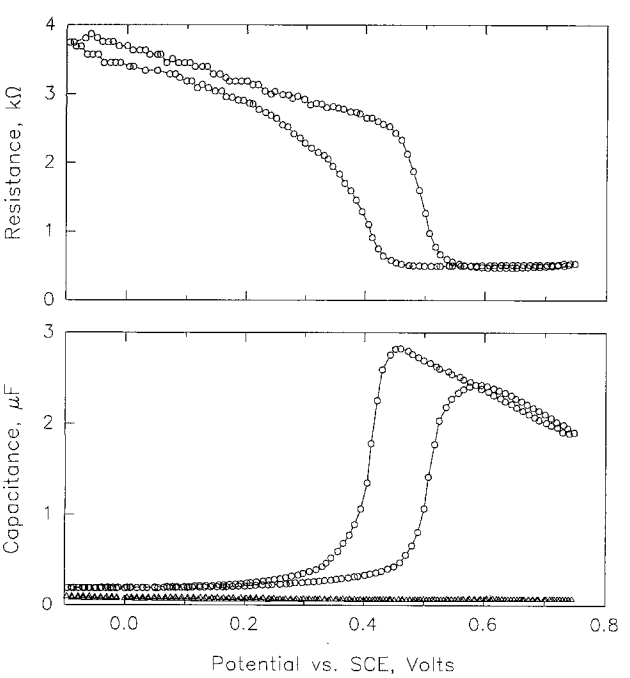

Fig. 6. Series resistance and capacitance of NiO film electrode (circles) and capacitance of uncoated Pt electrode (triangles). Electrode area 1.3 × 10^{-3} cm^2; sweep rate 1 mV/s; electrolyte 1*M* KCl + KOH, pH 12.0.

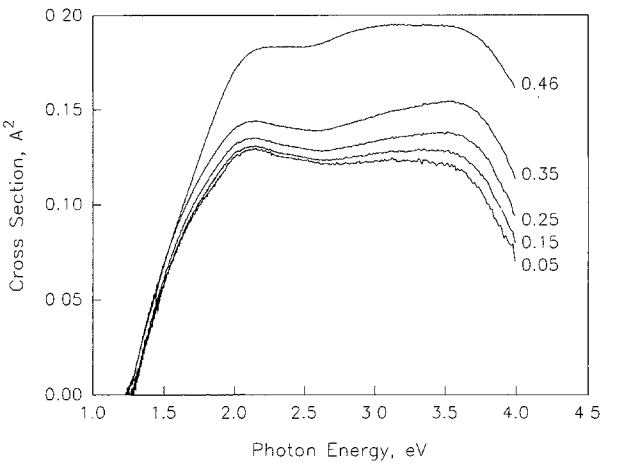

Fig. 7. Optical absorption cross section of an electrochromic NiO film at the indicated potential in V *vs.* SCE. The bleached state transmittance was measured at −0.15 V *vs.* SCE, and the electrolyte was 0.01*M* KOH.

pH behavior is seen for porous, hydrous oxides of Ir, Au, and Fe, and it has been suggested that the behavior may result from a hydrolysis-type reaction involving metal oxyhydroxide dimers.[40]

The optical absorption change of an electrochromic NiO film is shown in Fig. 7. About 0.3-7 a/o of the film was reduced, based on the transferred charge of 0.1-2 mC/cm^2. Clearly, a simple model of independent absorbing centers does not adequately describe the film behavior. The absorption per Ni(III) center becomes stronger as the film is oxidized, which suggests that interactions between the Ni(III) centers tend to enhance the optical absorption. Nearest-neighbor interactions are unlikely if the Ni(III) centers are uniformly distributed throughout the film volume; however, if the Ni(III) centers are concentrated at the grain surfaces, then there can be many neighboring centers. As the sample is bleached, the measurements approach a limiting spectrum, which is still very broad (about 2.5 eV in width), and may be composed of two broad subbands centered at about 2.0-2.1 eV and 3.4-3.5 eV. The large bandwidths suggest that the optical transitions are strongly coupled to vibrational modes, and this is seen in Raman scattering from oxidized $Ni(OH)_2$ films.[24]

Figure 8 shows XPS survey spectra with line assignments for the sample pair. The only elements detected were Ni, O, and C, which indicates that other elements (aside from H and He) were present at levels below about 0.5 a/o. The Ni 2p spectra (Fig. 9) for the bleached and colored states are essentially the same, and there is excellent correspondence to measurements on NiO samples.[41-43]

There are two O 1s peaks present (Fig. 10). Vacuum-cleaved NiO crystals show only the oxide peak at 529 eV; the additional peak at 1.8 ± 0.1 eV higher binding energy corresponds to the "adsorbate" peak seen for polycrystalline NiO and for oxygen adsorbed on NiO.[43] The electrochromic films have a large adsorbate component, between 40 and 80% of the total O 1s intensity. XPS measurements were made on two samples which were poorly electrochromic (charge transfer < 1 mC/cm^2 in the cell), and they each had <20% of the O 1s intensity in the adsorbate peak.

Based on intensity ratios for the Ni 2p and O 1s levels, the Ni:O ratio changes by less than 10% between the bleached and colored states. Thus, the electrode reaction is not associated with large changes in the number of oxygen atoms at the electrode surface. Some of the samples were ion bombarded with 3 keV Ar^+ in the XPS vacuum chamber. Ion bombardment tends to remove the adsorbate O 1s peak and enhance the oxide peak (Fig. 11). It also increases the Ni 2p: O 1s intensity ratio, which indicates that the grain surfaces are oxygen-rich compared to the grain interiors. Except for

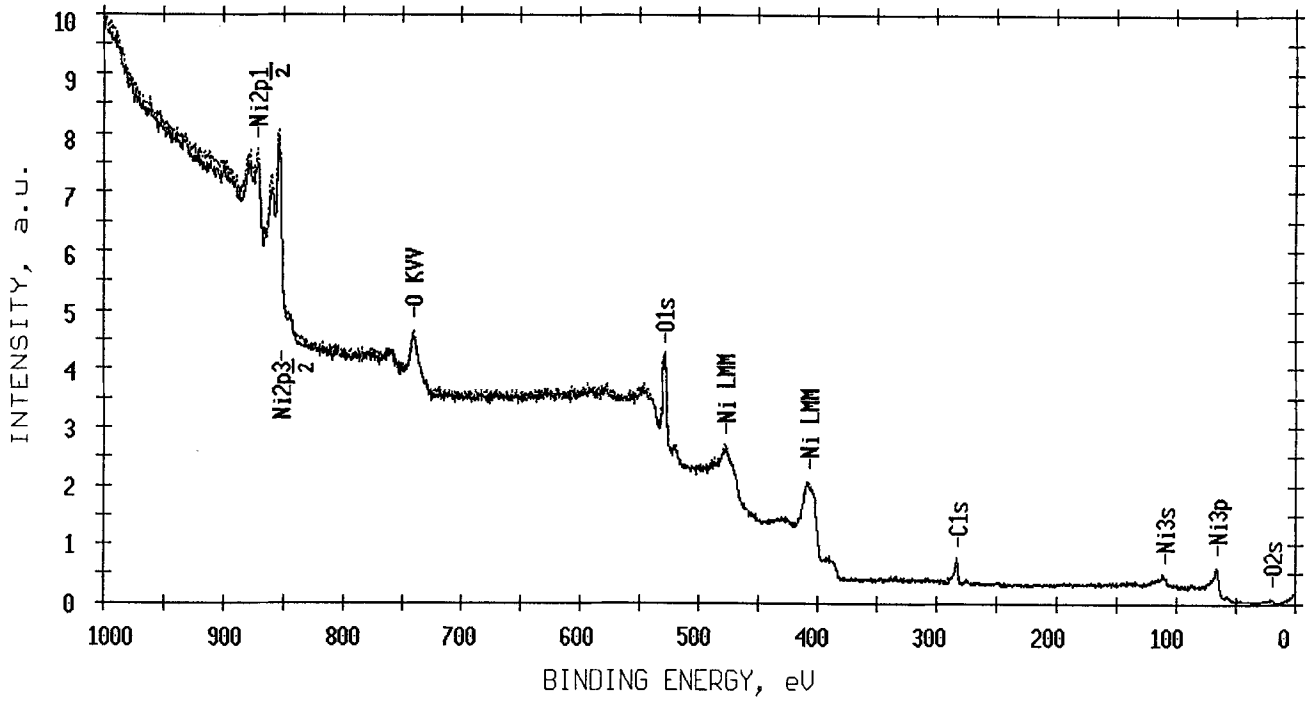

Fig. 8. XPS survey spectra for NiO film pair: dashed line, bleached state; solid line, colored state.

Fig. 11, the spectra reported here were taken before ion bombarding the sample.

Figure 12 shows the XPS spectra near the Fermi level. The energy resolution and count rate were rather poor for valence band studies, but the data are consistent with valence band spectra of polycrystalline NiO samples.[44-46] The electrode reaction is not accompanied by a large change in the density of states at the Fermi level, which is consistent with the dc resistivity measurements.

Discussion

The x-ray and infrared results indicate that the films retain the polycrystalline NiO structure when they are oxidized and reduced. The NiO grain interiors are expected to be chemically inactive, so the electrochromic reaction likely occurs at the grain boundaries. Treating the film as a homogeneous slab, the apparent surface area is in the range 0.1-1 m^2/g. The charge transferred during oxidation and reduction, on the assumption of 10^{15} singly charged species per cm^2, implies that the true surface area of the films is ≈70 m^2/g. The electrode capacitance data, assuming a capacitance of 10 $\mu F/cm^2$ (typical value at a metal electrode), indicates a true surface area of ≈100 m^2/g. These estimates are close to the surface area obtained by modeling the film grains as circular cylinders of diameter 10 nm (≈60 m^2/g), square pillars of side 10 nm (≈60 m^2/g), and cones with base diameter 10 nm (≈90 m^2/g).

The grain surfaces are oxygen-rich compared to the NiO cores. Here the most direct evidence is the increase in the Ni:O ratio after Ar^+ ion bombardment in the XPS chamber. Supporting evidence is provided by the partially oxidized state of as-grown films, which may result from adsorption

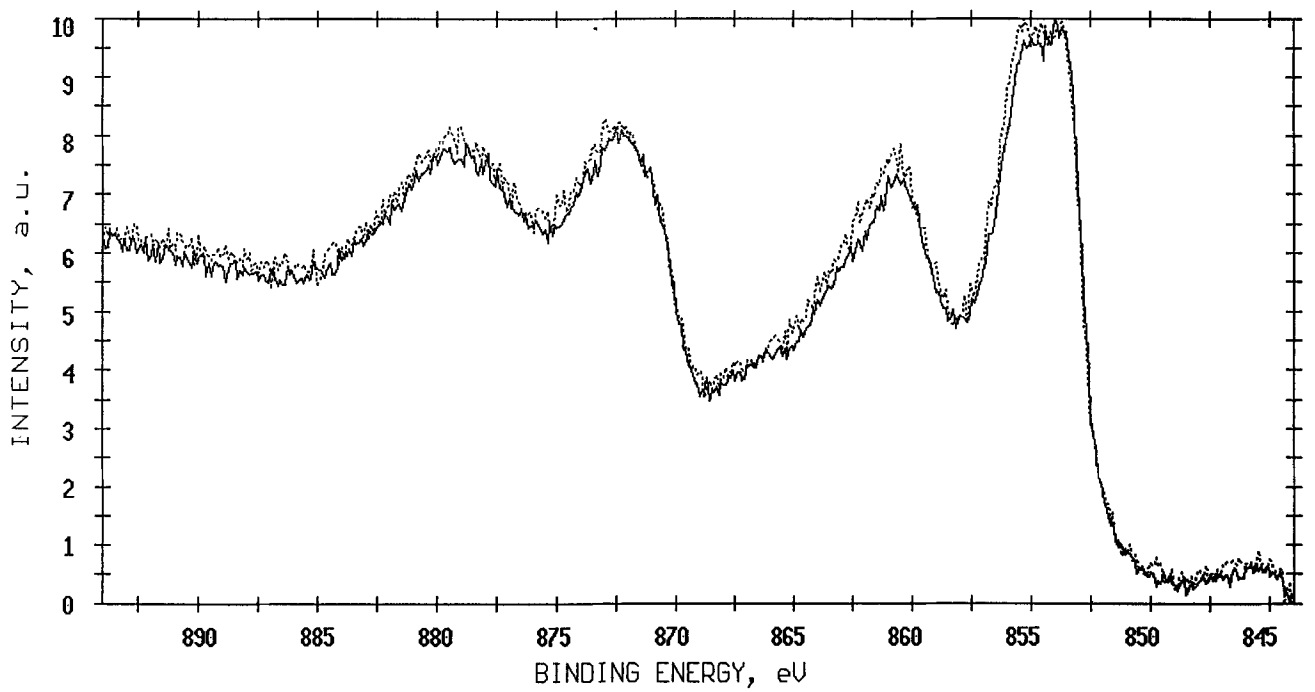

Fig. 9. XPS spectra for NiO film pair: dashed line, bleached state; solid line, colored state. Ni 2p region.

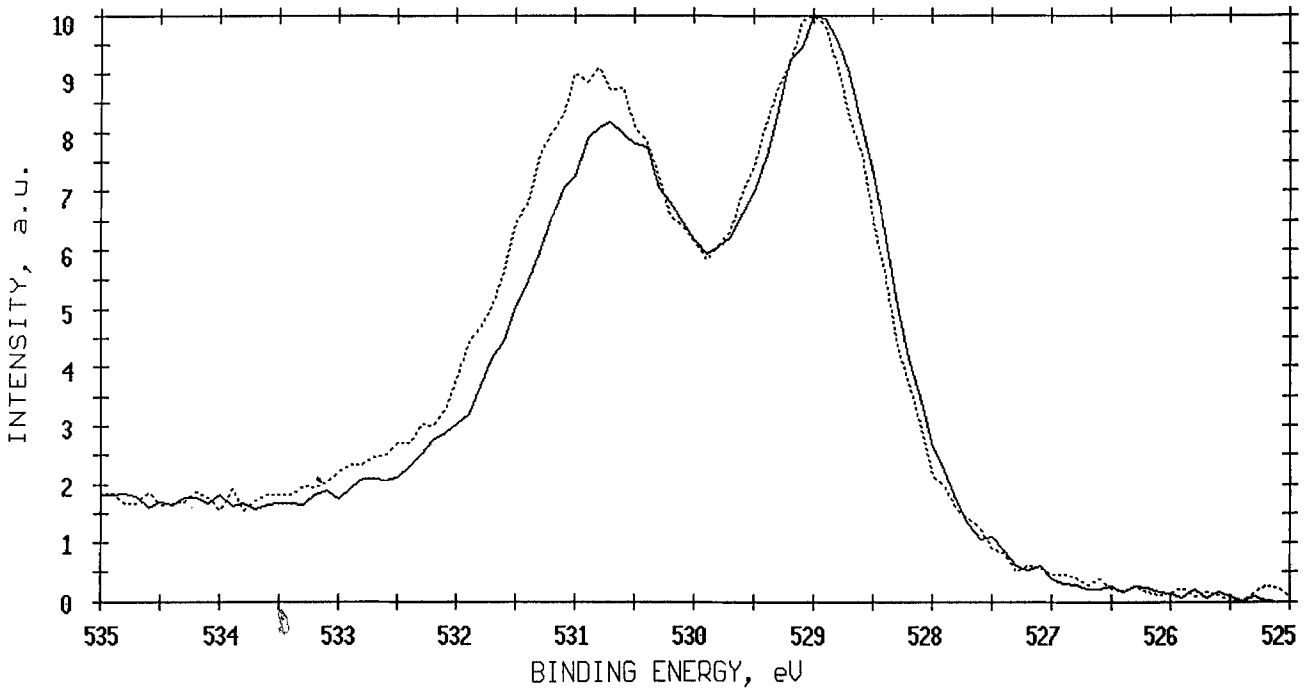

Fig. 10 XPS spectra for NiO film pair: dashed line, bleached state; solid line, colored state. O 1s region.

of O_2 and H_2O, and the effect of heat-treatments on the electrochemical response. It has been proposed that the electrochromic reaction in NiO films involves the direct adsorption and desorption of OH^- ions in the cell.[12,18] There is probably some irreversible adsorption of OH^- groups during the initial oxidation of the film, and OH^- ions at the outer Helmholtz plane certainly play a role, but the XPS results indicate that the electrochromic reaction proceeds with little or no change in the amount of adsorbed oxygen. Thus, it is far more likely that there is proton transfer at the solid/liquid interface.

A connection between film structure and reactivity can be made in the following qualitative fashion. O_2 and H_2O do not bond to the five-fold coordinated Ni^{2+} and O^{2-} ions on a cleaved NiO (100) surface.[43] On the electrochromic NiO films, however, many of the surface ions occupy low-coordination sites (coordination number 3 or 4) such as steps, corners, and small (111) terraces. The low-coordination ions have more electron density available for bonding to adsorbates, so the films can adsorb O_2 and H_2O, and H^+ and OH^- in the cell, to produce an oxygen-rich, hydroxylated film surface. When a film is dehydrated during the heat-treatment, there is a tendency for the number of five-fold sites to increase at the expense of the low-coordination sites, which lowers the surface energy. When returned to the cell, there are fewer active sites available, so the electrochemical response is smaller.

One of the main questions which remains to be answered for the electrochromic NiO films concerns the nature of the transitions which are responsible for the optical absorption in the colored films. We do not attempt a full answer here, but as a reasonable starting point, we consider the optical

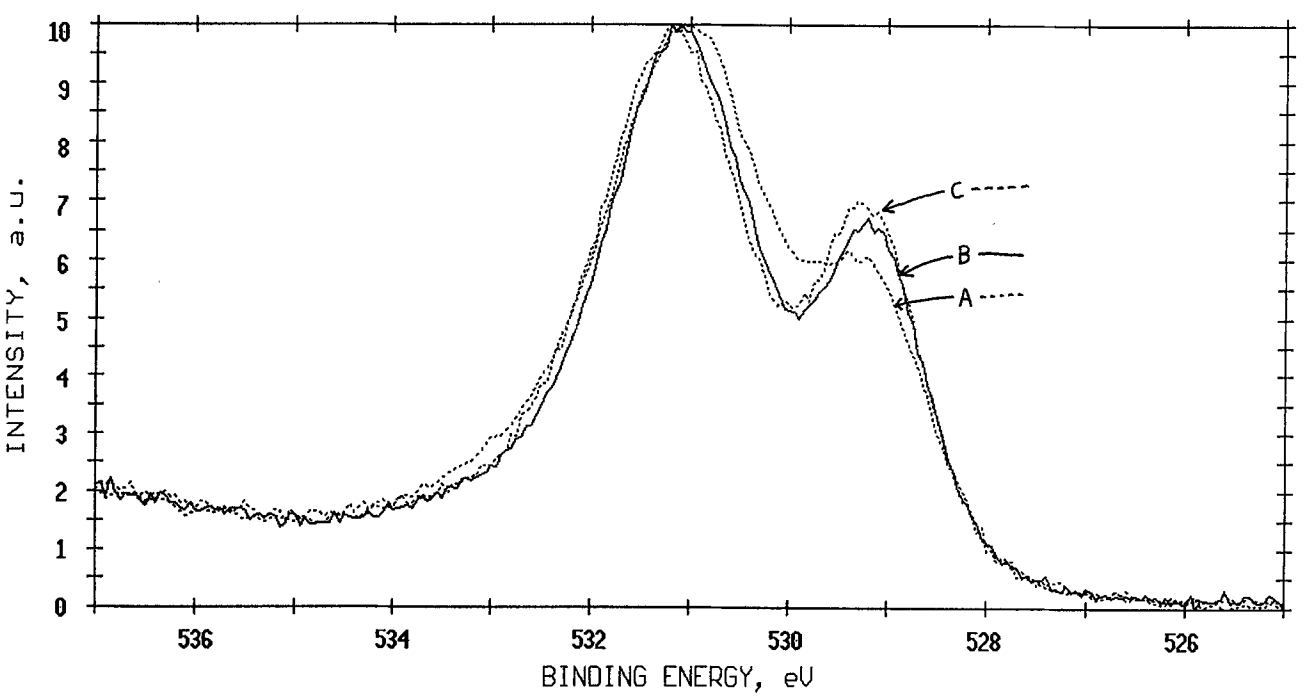

Fig. 11. O 1s region of XPS spectrum of a NiO film sample: A, before ion bombardment; B, after 1 min Ar^+ ion etch; after 2 min Ar^+ ion etch.

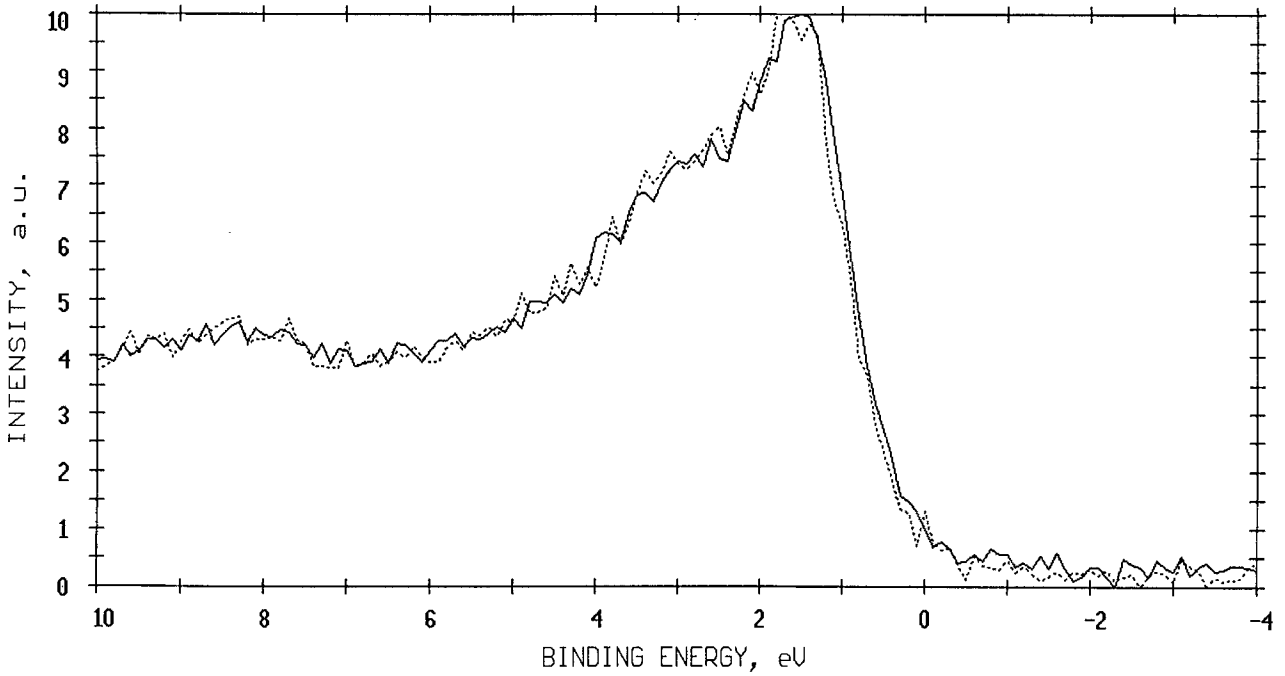

Fig. 12. XPS valence band spectra for NiO film pair: dashed line, bleached state; solid line, colored state.

transitions on an octahedral NiO_6 cluster. For a central Ni^{2+} ion surrounded by six O^{2-} ions, the optical behavior is similar to that of stoichiometric NiO or $Ni(OH)_2$. The minimum energy for strong absorption is about 4 eV, and corresponds to the "bandgap" transition $3d^8 \rightarrow 3d^9$ L, where L denotes a hole on an O^{2-} ligand (that is, an O^- ion).[47,48]

If the cluster is "oxidized" so that it now consists of a central Ni^{2+} ion surrounded by five O^{2-} ions and one O^- ion, two new absorption bands are expected, and these may account for the bands seen in Fig. 7. Transfer of the hole from one oxide ion to another results in optical absorption because the electronic transition is strongly coupled to the vibrational modes of the cluster. By analogy to O^- centers in MgO and CaO, the oxide to oxide transfer is expected to produce a broad absorption band centered at about 2 eV, which can be described in a configuration coordinate scheme.[49,50] The other new absorption band is associated with the transition $3d^8$ L $\rightarrow 3d^7$, which is expected to have an energy close to the "bandgap" value, and this may account for the 3.4-3.5 eV band in Fig. 7. Again, strong coupling to the vibrational modes of the cluster would produce a very broad absorption band. If the inhomogeneous broadening is not too large, the optical absorption mechanisms in the films may be studied by optical measurements at low temperatures.

Summary and Conclusions

The electrochromic response of NiO films is greatly reduced by modest heat-treatments, suggesting that this response is associated with easily removed defects at the grain boundaries. This hypothesis is supported by x-ray diffraction and IR absorption measurements on the films which indicate that there is no change in crystal structure when the films are oxidized and reduced in the electrochemical cell. The electronic properties and chemical behavior of sputtered electrochromic NiO films and electrodeposited electrochromic $Ni(OH)_2$ films are very similar which is not likely if the electrochromism were a bulk phenomenon. The behavior of the electrode resistance and capacitance also indicate a modification of the NiO surface during oxidation and reduction. Electrochromic activity appears to be correlated to excess adsorbed oxygen detected by XPS.

Based on the above observations, electrochromic activity requires a porous, granular NiO film with excess oxygen at the grain surfaces. Reduction of the film then results from the transfer of protons from water molecules to oxygen ions at the solid surface (proton adsorption), and oxidation of the film is due to transfer of protons from the solid surface to hydroxyl ions in solution (proton desorption). The colored state may be ascribed to electronic transitions from localized levels associated with the surface oxygen ions to empty levels on the oxygen ions or near the conduction bandedge. The probability of such a transition is much lower in the bleached film due to the formation of the O-H bonds at the film surface.

Acknowledgments

We would like to thank Neil Bartlett, Paul Berdahl, Frank Ogletree, and Carl Lampert for helpful discussions. This work was supported by the Assistant Secretary for Conservation and Renewable Energy, Office of Building Technologies, Building Systems and Materials Division of the U.S. Department of Energy under Contract No. DE-AC03-76SF00098.

Manuscript submitted July 29, 1992; revised manuscript received Dec. 21, 1992.

Lawrence Berkeley Laboratory assisted in meeting the publication costs of this article.

REFERENCES

1. J. P. Hoare, *The Electrochemistry of Oxygen,* pp. 271-293, Wiley-Interscience, New York (1968).
2. G. W. D. Briggs, in *A Specialist Periodical Report: Electrochemistry,* Vol. 4, H. R. Thirsk, Editor, p. 33, The Chemical Society, London (1974).
3. P. Oliva, J. Leonardi, J. F. Laurent, C. Delmas, J. J. Braconnier, M. Figlarz, F. Fievet, and A. de Guibert, *J. Power Sources,* **8,** 229 (1982).
4. R. G. Gunther and S. Gross, Editors, *The Nickel Electrode,* The Electrochemical Society Softbound Proceedings Series, PV 82-4, Pennington, NJ (1982).
5. D. A. Corrigan and A. H. Zimmerman, Editors, *Nickel Hydroxide Electrodes,* The Electrochemical Society Softbound Proceedings Series, PV 90-4, Pennington, NJ (1990).
6. C. M. Lampert, T. R. Omstead, and P. C. Yu, *Solar Energy Mater.,* **14,** 161 (1986).
7. J. S. E. M. Svensson and C. G. Granqvist, *Appl. Phys. Lett.,* **49,** 1566 (1986).
8. P. C. Yu, G. Nazri, and C. M. Lampert, *Solar Energy Mater.,* **16,** 1 (1987).
9. M. K. Carpenter, R. S. Conell, and D. A. Corrigan, *ibid.,* **16,** 333 (1987).
10. M. Fantini and A. Gorenstein, *ibid.,* **16,** 487 (1987).
11. J. S. E. M. Svensson and C. G. Granqvist, *Appl. Opt.,* **26,** 1554 (1987).
12. P. Delichere, S. Joiret, A. Hugot-Le Goff, K. Bange, and B. Hetz, *This Journal,* **135,** 1856 (1988).
13. W. Estrada, A. M. Andersson, and C. G. Granqvist, *J. Appl. Phys.,* **64,** 3678 (1988).

14. S. Yamada, T. Yoshioka, M. Miyashita, K. Urabe, and M. Kitao, *ibid.*, **63,** 2116 (1988).
15. D. A. Corrigan and S. L. Knight, *This Journal,* **136,** 613 (1989).
16. M. K. Carpenter and D. A. Corrigan, *ibid.*, **136,** 1022 (1989).
17. S. Passerini, B. Scrosati, A. Gorenstein, A. M. Andersson, and C. G. Granqvist, *ibid.*, **136,** 3394 (1989).
18. S. I. Cordoba-Torresi, A. Hugot-Le Goff, and S. Joiret, *ibid.*, **138,** 1548 and 1554 (1991).
19. D. A. Wruck, M. A. Dixon, M. Rubin, and S. N. Bogy, *J. Vac. Sci. Technol. A,* **9,** 2170 (1991).
20. C. M. Lampert, *Solar Energy Mater.,* **11,** 1 (1984).
21. C. M. Lampert and C. G. Granqvist, Editors, *Large Area Chromogenics: Materials and Devices for Transmittance Control,* SPIE, Bellingham, WA (1990).
22. R. S. McEwen, *J. Phys. Chem.,* **75,** 1782 (1971).
23. F. von Sturm, in *Comprehensive Treatise of Electrochemistry,* Vol. 3, J. O'M. Bockris, B. E. Conway, E. Yeager, and R. E. White, Editors, p. 385 (1981).
24. J. Desilvestro, D. A. Corrigan, and M. J. Weaver, *J. Phys. Chem.,* **90,** 6408 (1986) and *This Journal,* **135,** 885 (1988).
25. K. I. Pandya, W. E. O'Grady, D. A. Corrigan, J. McBreen, and R. W. Hoffman, *J. Phys. Chem.,* **94,** 21 (1990).
26. A. Bielanski and M. Najbar, *J. Catal.,* **25,** 398 (1972).
27. J. A. Thornton, *J. Vac. Sci. Technol.,* **11,** 666 (1974) and **12,** 830 (1975).
28. A. J. Bard, A. B. Bocarsly, F. F. Fan, E. G. Walton, and M. S. Wrighton, *J. Am. Chem. Soc.,* **102,** 3671 (1980).
29. D. Adler and J. Feinleib, *Phys. Rev. B,* **2,** 3112 (1970).
30. H. A. Macleod, *Thin-Film Optical Filters,* pp. 368-381, Macmillan, New York (1986).
31. D. W. Berreman, *Phys. Rev.,* **130,** 2193 (1963).
32. W. Reichardt, V. Wagner, and W. Kress, *J. Phys. C,* **8,** 3955 (1975).
33. R. Ruppin and R. Englman, *Rep. Prog. Phys.,* **33,** 149 (1970).
34. A. J. Hunt, T. R. Steyer, and D. R. Huffman, *Surf. Sci.,* **36,** 454 (1973).
35. D. A. Wruck, Ph.D. Thesis, University of California, Berkeley (1991).
36. A. A. Tsyganenko, T. A. Rodionova, and V. N. Filimonov, *React. Kinet. Catal. Lett.,* **11,** 113 (1979).
37. M. Che and A. J. Tench, *Adv. Catal.,* **32,** 1 (1983).
38. Y. Takita, Y. Saito, T. Tashiro, and F. Hori, *Bull. Chem. Soc. Jpn.,* **58,** 1827 (1985).
39. M. J. Natan, D. Belanger, M. K. Carpenter, and M. S. Wrighton, *J. Phys. Chem.,* **91,** 1834 (1987).
40. L. D. Burke and D. P. Whelan, *J. Electroanal. Chem.,* **124,** 333 (1981) and **162,** 121 (1984).
41. K. S. Kim and R. E. Davis, *J. Electron Spectrosc.,* **1,** 251 (1972).
42. K. S. Kim and N. Winograd, *Surf. Sci.,* **43,** 625 (1974).
43. J. M. McKay and V. E. Henrich, *Phys. Rev. B,* **32,** 6764 (1985).
44. M. D. Rechtin and B. L. Averbach, *J. Phys. Chem. Solids,* **36,** 893 (1975).
45. S. Kowalczyk, L. Ley, R. Pollack, and D. Shirley, data on p. 731 of B. H. Brandow, *Adv. Phys.,* **26,** 651 (1977).
46. G. A. Sawatzky and J. W. Allen, *Phys. Rev. Lett.,* **53,** 2339 (1984).
47. A. Fujimori and F. Minami, *Phys. Rev. B,* **30,** 957 (1984).
48. J. Zaanen, G. A. Sawatzky, and J. W. Allen, *Phys. Rev. Lett.,* **55,** 418 (1985) and *J. Magnet. Magnet. Mater.,* **54/57,** 607 (1986).
49. O. F. Schirmer, K. W. Blazey, W. Berlinger, and R. Diehl, *Phys. Rev. B,* **11,** 4201 (1975).
50. M. J. Norgett, A. M. Stoneham, and A. P. Pathak, *J. Phys. C,* **10,** 555 (1977).